Final Report

"Dynamical Studies of the Middle Atmosphere Using High Resolution Doppler Imager Observations"

NASA grant NAG5-11068
UM number F004998

Wilbert Skinner, P.I.

Introduction

This report summarizes the activities of NASA grant NAG5-11068, "Dynamical Studies of the Middle Atmosphere Using High Resolution Doppler Imager Observations."

HRDI Summary

The High Resolution Doppler Imager (HRDI) on the Upper Atmosphere Research Satellite (UARS) (Reber, 1990, Schoeberl et al., 1994) has been providing direct measurements of the Earth's horizontal wind field in the stratosphere, mesosphere and lower thermosphere. Mesospheric temperatures, ozone, and $O(^1D)$ densities, and stratospheric aerosol extinctions coefficients, are also retrieved. The goal of HRDI is to measure the vector winds in the stratosphere (10-40 km), mesosphere, and lower thermosphere (~50-120 km) during the day, and the lower thermosphere at night (~95 km) to an accuracy of 5 m/s. The horizontal wind vector is measured by observing the Doppler shift of rotational lines of molecular oxygen along two lines of sight (Hays, 1982, Abreu et al., 1989, Hays and Abreu, 1989, Hays et al., 1993, Grassl et al., 1995, Skinner et al., 1994, 1996, 1999, 2003). In addition to winds, temperatures and volume emission rates are determined in the mesosphere and lower thermosphere, from which ozone and $O(^1D)$ concentrations can be derived, and aerosol scattering coefficients are determined in the stratosphere. UARS was launched on September 12, 1991, into a 585-km circular orbit inclined 57° to the equator HRDI was activated September 28, 1991 and following a period of checkout and adjustment of the instrument parameters, scientific observations began November 2, 1991. HRDI operated nearly continuously from launch until April 1995. At that time the UARS solar array drive failed, forcing the instruments to time-share the available power. From July 1995 to July 1996 HRDI operated approximately 50% of the time. At that point, one of the three spacecraft batteries failed and from then until September 1998 the duty cycle was less than 20% per month, At that time it was determined that HRDI could operate during each daytime pass, which increased the daytime duty cycle to close to 100%, while nighttime operations were limited to about a week per month. In the fall of 1999, the second tape recorder failed requiring a real time contact with a TRDSS satellite to retrieve that data. This resulted in about 60% data collection efficiency. Finally, in the summer of 2000, the second star sensor failed requiring the spacecraft attitude to be controlled by a three axis magnetometer and sun sensor. This resulted in a loss of attitude knowledge but operations continue with the anticipation of correcting the attitude.

A Data Assimilation Technique for Determining Tidal and Zonal Mean Structure from Satellite Measurements in the Mesosphere and Lower Thermosphere

A new method for determining the tide and mean structure from satellite data in conjunction with a new tidal model has been devised. For brevity, it shall be referred to as the TMAT or Tide-Mean Assimilation Technique. Most previous methods of tidal analysis are based on various ways of slicing the data set. For example, one could collect

a set of data at a fixed latitude and altitude and perform a spectral analysis in local time of a each measured field (u, v or T). Various other ways of slicing through the data set are illustrated in the first set of figures.

The TMAT is based on the premise that adequate information on tide and mean state components can be obtained by simultaneously considering the latitude-altitude structure of all three fields from a single day's worth of measurements. In other words, the 'slice' of data taken on any given day is considered. It is commonly considered that the latitude-altitude structure of a combination of tides and mean state as observed by satellites such as UARS or TIMED is inseparable on a daily basis. In fact, this combination is not completely arbitrary, and the dynamical constraints provided by thermal wind balance and the tidal equations can be used to separate the components. In essence, *the TMAT uses the latitude-altitude structure of the observations, rather than the local time structure, to determine he tidal and zonal mean structure.* The TMAT is similar to normal mode initialization procedures used in time-dependent assimilation models, but rather than projecting observations onto 'slow' modes, they are projected onto a combination of geostrophic modes and tidal modes. Since the concept of projection underlies all fitting techniques, the TMAT can therefore be viewed as a fit of a tide and mean state model to the observations.

There are several potential advantages of the TMAT over the methods previously used with HRDI or WINDII/UARS data:

• *The TMAT can separate the tides and the mean state components on a daily basis.* Thus, information on tidal and mean state variability on less than the seasonal time scale can be obtained. There is evidence from radar measurements that tidal amplitudes vary on a weekly time scale, and it is likely that the mean state can vary on a similar time scale.

• *The residual of the tide-mean fit to the data will contain information on the meridional circulation and any other ageostrophic states.*

• *The TMAT can provide estimates of the structure of tidal forcing.* Part of the tidal fit will include the amplitudes of various tidal modes, and in analogy with classical tidal theory, these arise from the structure and strength of the forcing regions below the MLT. The fit will also include a parameterization of the damping structure, and thus provides information on gravity wave stress and diffusion within the MLT.

Data Assimilation Method.

The TMAT employs linear perturbation techniques as well as Newtonian iteration to achieve a fit of a tidal and zonal mean model to the data. This means that the tidal model must be run many times in order to compute the perturbations with respect to several parameters. A fast and accurate model is therefore required, and a new tidal model was developed with this in mind. This model uses the method of multiple scales and a simple shooting method to solve the Laplace tidal equations. For brevity, the tidal model used here will be called the MSTM, for Multiple Scales Tidal Model. Besides the tidal model, two other models are required for the TMAT - a mean state model and a gravity wave stress model.

• The mean state model consists of a finite set of thermal wind modes which are constructed in terms of the zonal mean horizontal stream function. Wind and temperature field are determined from this. The stream function is represented in both latitude and

altitude in terms of Legendre polynomials. 90 basis functions are used, which is adequate for reproducing the CIRA climatology quite well.

- An effective Rayleigh friction coefficient α is used to represent the effects of gravity wave breakdown on tides. This coefficient is allowed to be complex;. A distinct coefficient is applied separately to each wind component and temperature. The functional dependence of α on latitude and altitude is given by

$$\alpha(\phi, z) = A \exp(-((\phi - \phi_0) / \Delta\phi)^2 - ((z - z_0) / \Delta z)^2,$$

and different values of the parameters apply to each hemisphere.

Tidal Model.

As in classical tidal theory, a general solution of the tidal equation will be expressed by the MSTM in terms of a linear combination of tidal modes. Tidal modes can be utilized as a conceptual tool for understanding solutions to the non-separable tidal equations in two ways. First, a non-separable solution can be expanded in terms of classical Hough functions at each level. Because of the non-separability, the expansion coefficients will change from level to level. This is one manifestation of what is often referred to as mode coupling. Alternately, the tidal equations could be solved with a classical Hough function imposed as the lower boundary condition. The non-separability of the equation will cause the latitude structure of the solution to change with altitude. The MSTM provides solutions of this type. Rather than incorporating classical Hough modes, the MSTM modes are solutions to a particular horizontal structure equation at each individual altitude level. The decomposition of tidal solutions in terms of modes is also expedient for the TMAT, since the coefficients of this expansion are included among the fitting parameters.

The MSTM finds a solution to the primitive equations on the sphere linearized about an arbitrary zonal mean state. The domain of interest is the altitude range from 60 to 120 km, and it is assumed that the tidal structure is predominantly determined by thermal forcing below this region. Forcing within the MLT is parameterized solely by frictional damping of the form $X' = -\alpha_1(\phi,z)u'$, $Y' = -\alpha_2(\phi,z)v'$, $Q' = -\alpha_3(\phi,z)T'$, and where the damping coefficients are as described in the previous section. The lower boundary condition is specified in terms of the geopotential, and the radiation condition is imposed at the upper boundary.

A single partial differential equation for geopotential may be obtained from the linearized perturbation equations by elimination of the horizontal and vertical wind fields. This equation is a non-separable PDE in ϕ and z for general damping and mean winds - the non-classical tidal equation. This equation is typically solved by using a method of Lindzen and Kuo (1969).

Approximate solutions to the non-classical tidal equations are obtained via a perturbation method that is an extension of the multiple scales solution method pioneered by Lindzen (1971) for the study of equatorial planetary waves and greatly simplified by Andrews and McIntyre (1976) and Boyd (1978). The only effect not contained at lowest order in the MSTM perturbation expansion is vertical shear of the mean state fields, and this assumption is all that is needed to allow the lowest order equations to remain separable.

The eigenvalue problem that results depends on altitude and is easily and quickly solved via the shooting method. Accurate results are obtained with 200 latitude grid points. It is noteworthy that the shooting method used here does not have any problems whatsoever with inertial latitudes or numerical instability as long as none of the grid points are located exactly at an inertial latitude. These roots are well known as 'apparent' singularities of the geopotential equation and arise only because the original system of equations has been reduced to one equation via elimination. True singularities of the system only occur at critical latitudes.

In summary,

- The MSTM provides a computationally fast and trouble-free method of solving the non-classical tidal equations;
- In this method, the horizontal structure and vertical wavelength are allowed to vary slowly with altitude;
- a general solution is easily expressed as a linear combination of naturally defined modes.

Validation.

Several experiments have been performed to test the tidal model and the assimilation scheme. First, to examine the accuracy of the approximation methods used in the MSTM, an attempt was made to reproduce the tidal structure as computed by the GSWM98 (Hagan, 1999).

To begin, an initial guess at the damping coefficients was made and the resulting MSTM tidal structures computed for five modes of the diurnal or semi-diurnal tide. Next, perturbations of this structure were computed by varying several of the damping coefficient parameters. Standard least-squares fitting formulae were then applied to fit MSTM to GSWM. A very good fit was achieved to both the GSWM diurnal and semi-diurnal tide with the MSTM - the phase structure, amplitude growth with altitude and hemispheric asymmetries were all accurately reproduced. This indicates that only a few MSTM modes can efficiently reproduce the output of a non-separable 2D PDE solver such as the GSWM. (Figure 1.)

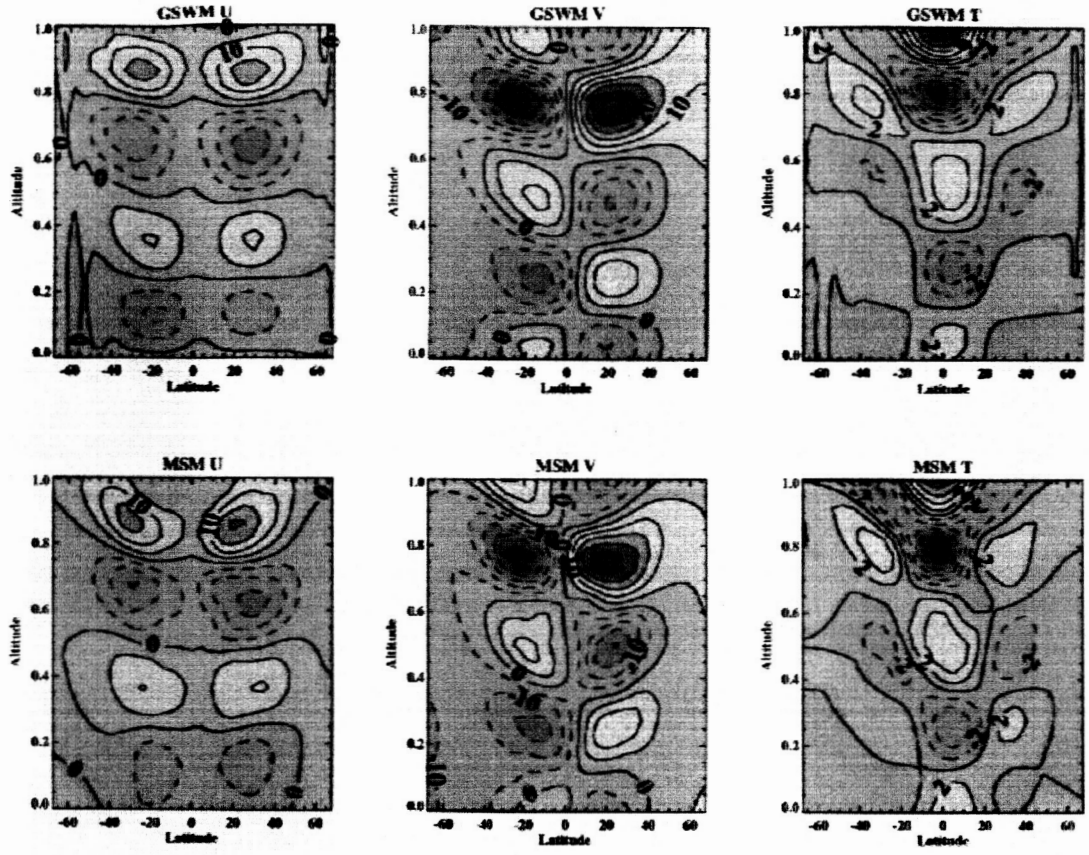

Figure 1

In the next experiment the full scope of the TMAT was tested. A day was chosen when HRDI made observations on both sides of the UARS orbit. The sampling pattern is shown in the upper left panel of Figure 2. This pattern is very similar to what will be produced by TIDI/TIMED measurements, and reflects day-time measurements only. Simulated measurements were formed from the CIRA climatology for January and the GSWM simulations of the diurnal and semi-diurnal tides for the same period. The structure that would be seen from HRDI in each of these three components and for the two separate tangent point tracks are shown in the plots of the first column of Figure 2.

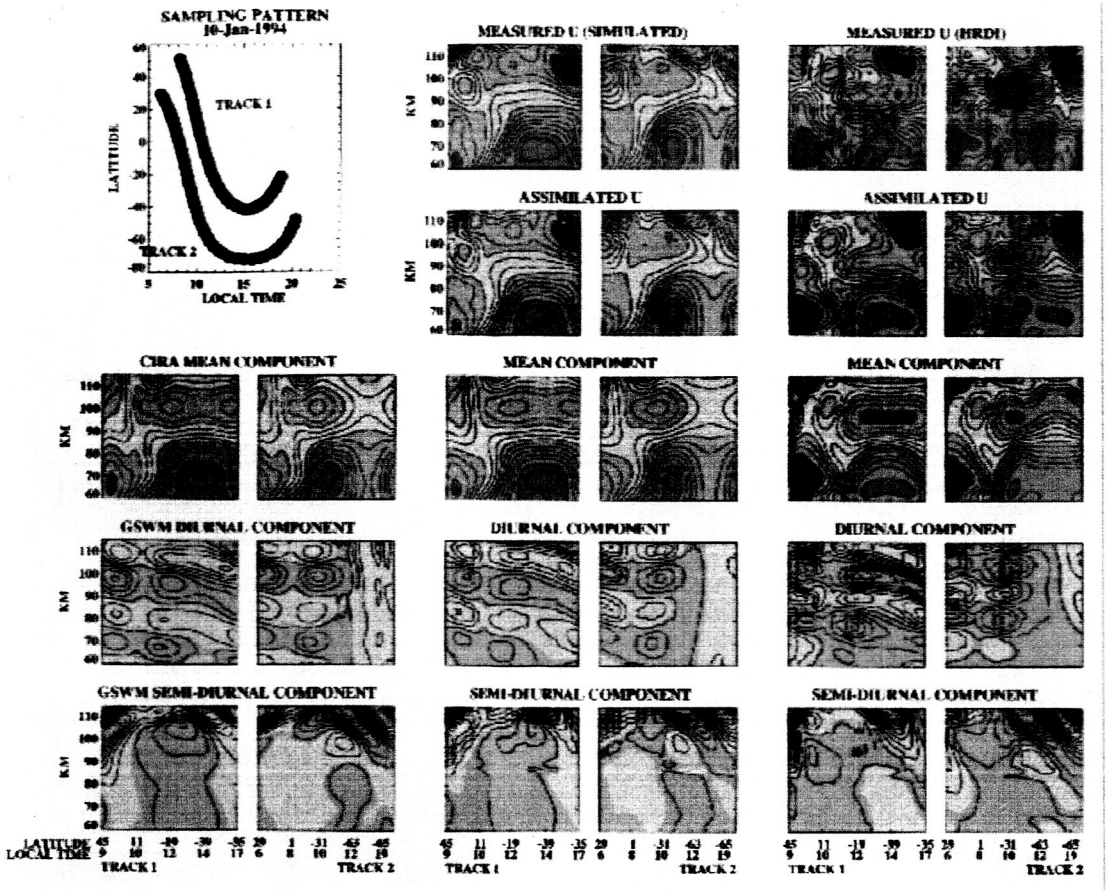

Figure 2

The superposition of the three fields shown in the first column is shown at the top of the next column. This represents the simulated measurements, and can be compared to actual HRDI measurements shown at the top of the third column. The next figures in the second and third columns show the results of assimilating either the simulated or HRDI measurements into the TMAT model. As can bee seen, the fit is remarkably good.

The resolution of the tide and mean components by the TMAT is shown in the remainder of the plots in the second and third column. The superposition of these three components gives the second plot of each column. The components shown in the second column can be compared directly to the originals in the first column. These figures compare extremely well with the original CIRA and GSWM fields, and demonstrate the power and flexibility of the TMAT. *A key feature of this experiment is that the simulated data was not produced by the same model that was used in the fit.*

The last column of Figure 2 shows the results of applying TMAT to HRDI measurements. Of course in this case there is no prior knowledge of the true state in which to compare the resolved components. It is interesting, however, to compare the results with the CIRA climatology and GSWM model. The mean and semi-diurnal components deduced by HRDI are qualitatively very similar to the CIRA and GSWM. The mean state seen by HRDI has the same easterly and westerly jet structure, except that there is an small easterly jet over the equator at 100 km. This is actually a chronic feature

in HRDI data and appears to be a facet of the MLT climatology missed by CIRA. The diurnal tidal amplitude seen by HRDI on this day appears to be somewhat stronger than the GSWM amplitude, and the phase is significantly shifted. The semi-diurnal tidal structures are in remarkably good agreement.

Much of the information used to obtain the tidal structure is contained in the meridional wind measurements (Figure 3), but some is also contained in the differences between the measurements of u and T from the two tracks in a complicated way. Figure 3. shows how tidal information is carried in the v field. This figure is rearranged slightly from Figure 2, so that the GSWM fields are shown in the middle column. The simulated v measurements are the sum of the two GSWM tidal components, and the TMAT resolution of these two components is shown in the first two rows of the first column. The TMAT resolution of the tidal components in HRDI data is shown at the top of the third column. The bottom plot in columns 1 and 3 show the respective fits of the TMAT to the two measurement sets. The fit is almost perfect in the case of the model simulation because no meridional circulation was included. The last plot in the second column shows the residual between HRDI measurements and the model fit. It reveals some of the structure in the mean meridional wind. Although there appears to be some slight residual of the tides due to the imperfect model fit, the structure at the right of the track 2 plot shows the expected equatorward winds arising from the gravity wave forcing in the southern summer hemisphere that produces the cold summer mesopause and jet reversal. Steady southward velocities are seen to occur throughout the lower thermosphere.

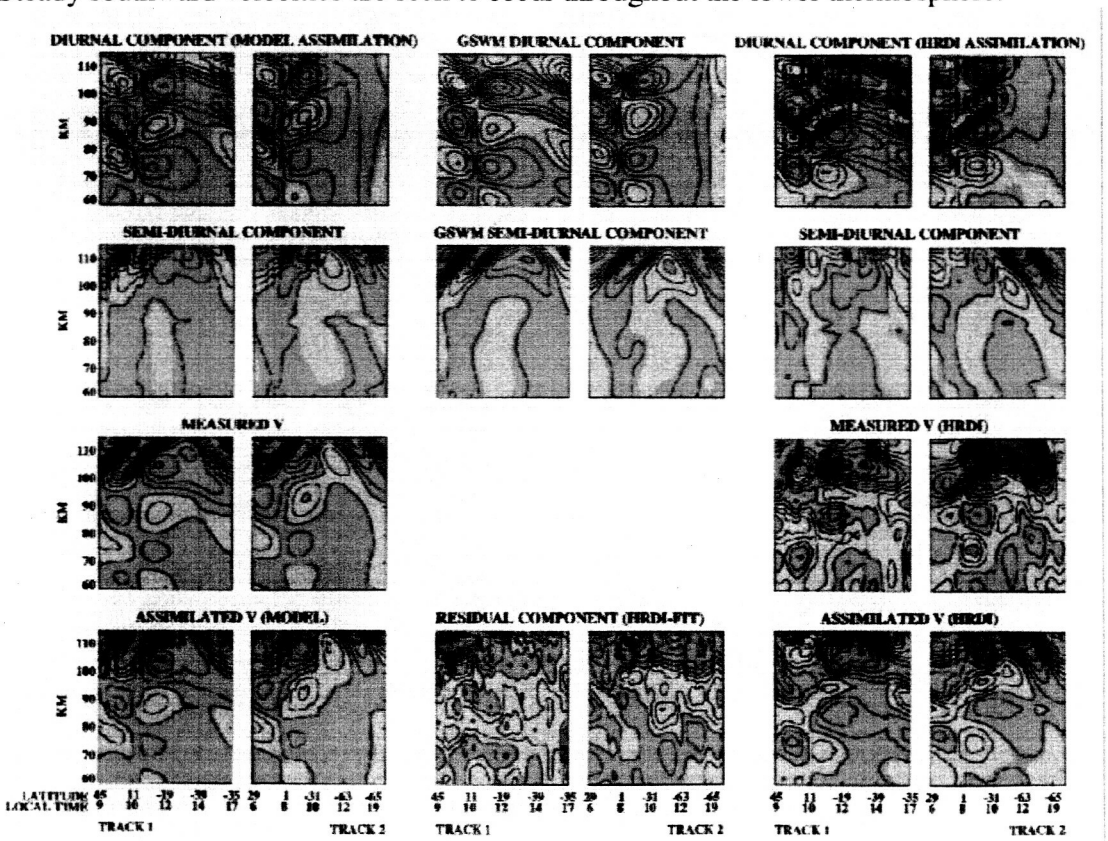

Figure 3

The results of the TMAT can be used to reconstruct the tide and mean state on any grid. A more typical display of the mean and tidal fields are shown in Figure 4 for the latitude range covered by HRDI on that day and at local midnight for the tide. This figure makes it a little easier to see the tide and mean state structure, and once again shows how well the TMAT reproduces the input in the simulated case and how the HRDI results compare with the climatology and model.

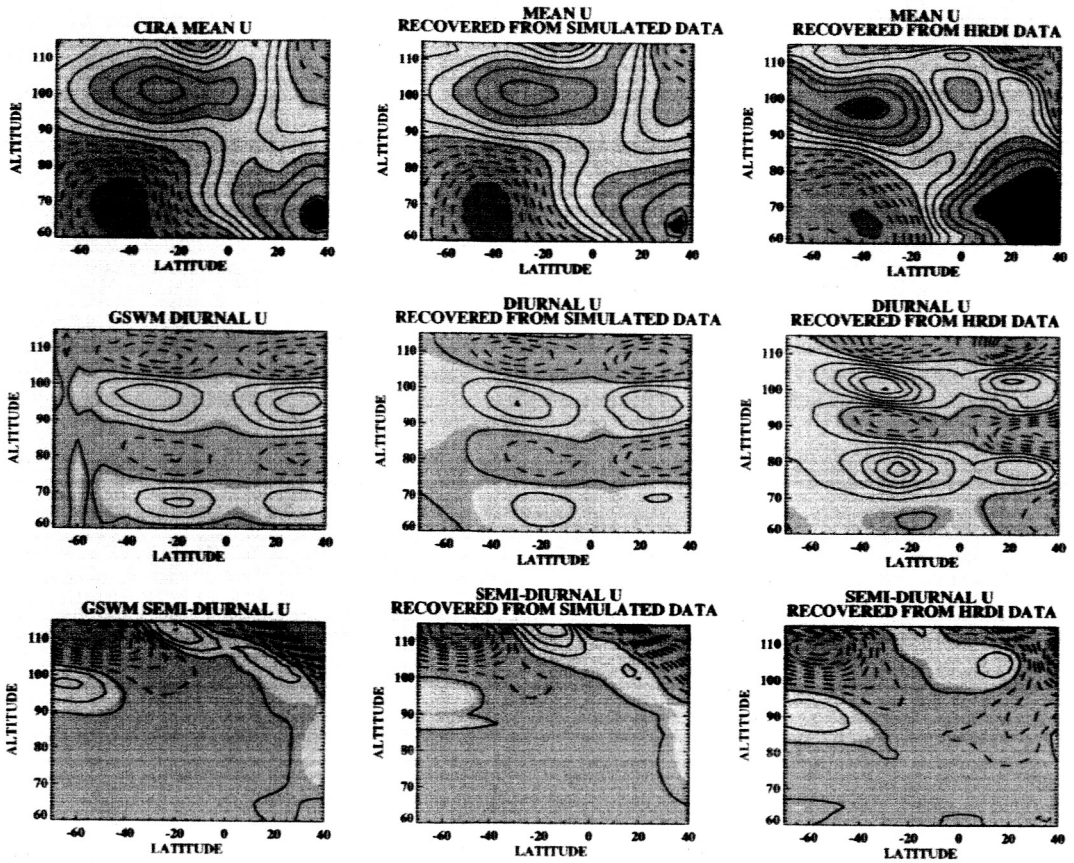

Figure 4

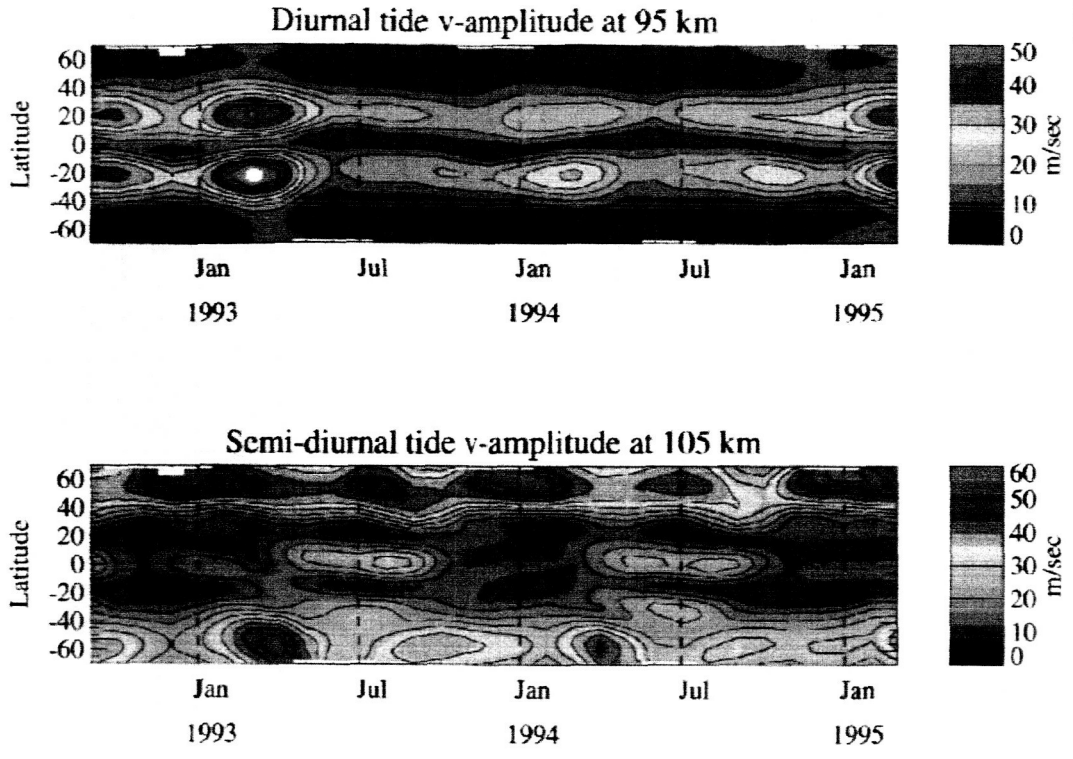

Examination of Forcing Mechanisms that act on the MLT with time scales longer than a year

It is well known that the MLT region shows very repeatable patterns from year to year. For example, the diurnal tide amplitude maximize at the equinox. In addition, there are very significant variations from year to year (e.g. Hagan et al. 1999). This study used meridional winds at 20 degrees north latitude from November 1991 to September 2000 as measured by the High Resolution Doppler Imager (HRDI). The purpose of this study is to look for possible forcing mechanisms such as:

–Solar (proxy: F10.7 index)
–Quasi-Biennial Oscillation (QBO) (proxy: zonally averaged equatorial zonal wind at 10 mb from UKMO assimilation model)
–Stratospheric aerosol (proxy: stratosphere optical depth from SAGE measurements at ~500 nm).
The data coverage and the proxies for the forcing mechanisms are shown in Figure 5.

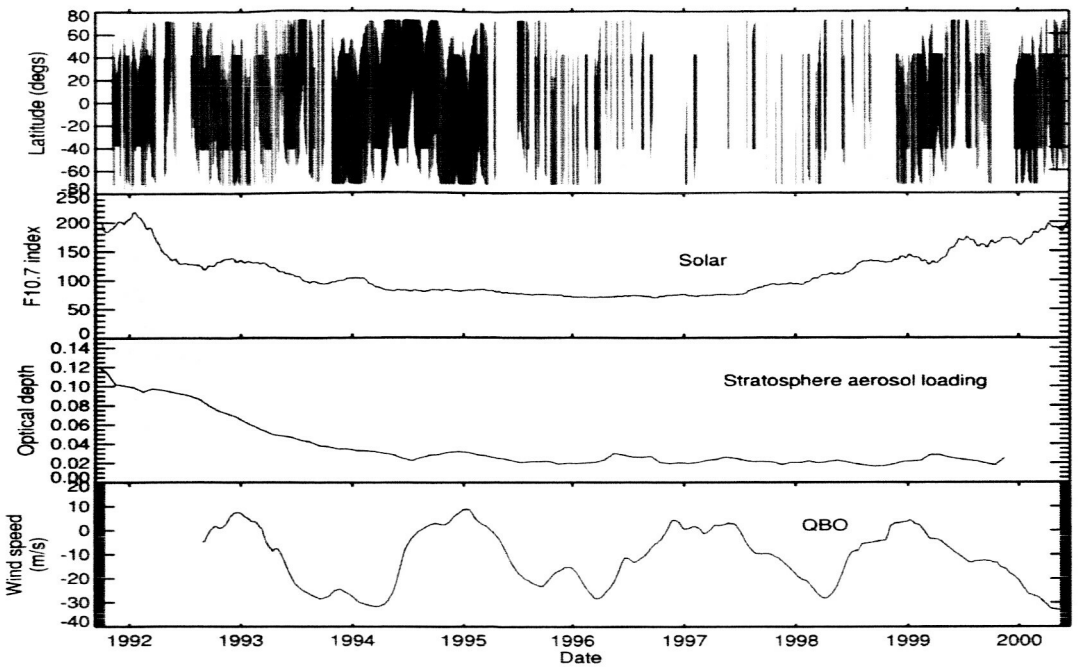

Figure 5. Illustration of the data used in this study. The top panel shows the daily latitude coverage of HRDI data during the UARS mission up to 2001. The second panel shows the mean F10.7 index which is used as a proxy for solar activity. Clearly shown is the two solar maximum periods that are encompassed in this study. The third panel shows the optical depth of the stratospheric aerosol at low latitudes. At the beginning the stratosphere was loaded with aerosols from Mt. Pinatubo while in later years the stratosphere has become quite clean. The bottom panel shows the zonally averaged zonal wind at 10 mb from the UKMO assimilation model which is used as a proxy for the QBO.

The data were binned in yaw cycle (approximately monthly) latitude, altitude, and local time bins. For the latitude of interest the binned altitude – local time winds were fit to: Each yaw cycle fit separately

$$V(z,t_{lt}) = V_{mean}(z) + V_{diurnal}(z)\cos\left(2\pi\left(\frac{z-z_{ref}}{z_w}+\frac{t_{lt}}{24}\right)+\omega\right)$$

where V_{mean}, $V_{diurnal}$ are the mean wind and diurnal tide amplitude as function of altitude and vertical wavelength z_w and phase ω. The variables V_{mean} $V_{diurnal}$ are constrained to be correlated with altitude and $V_{diurnal}$ constrained to have non-negative values

An example of the fit is shown in Figure 6 for a month near solstice, with the fit parameters shown in Figure 7 and a case near equinox shown in Figure 8 and Figure 9. The increase in the tidal amplitude near equinox is clearly evident.

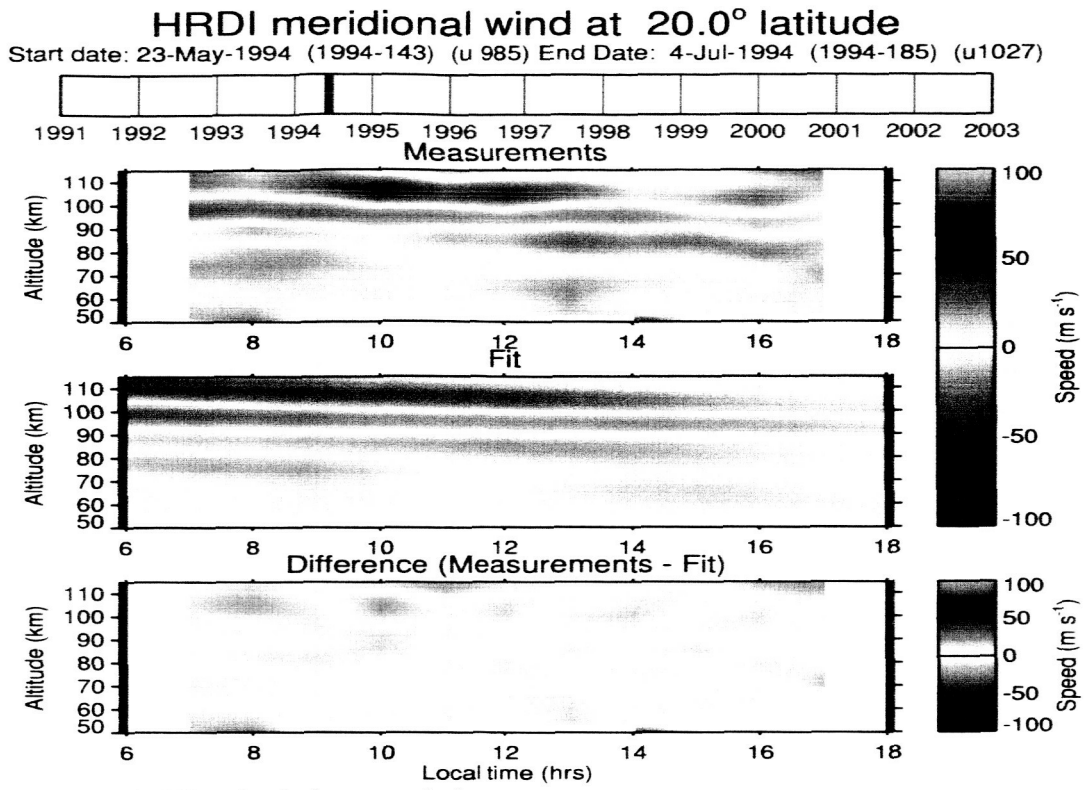

Figure 6. Meridional winds near solstice

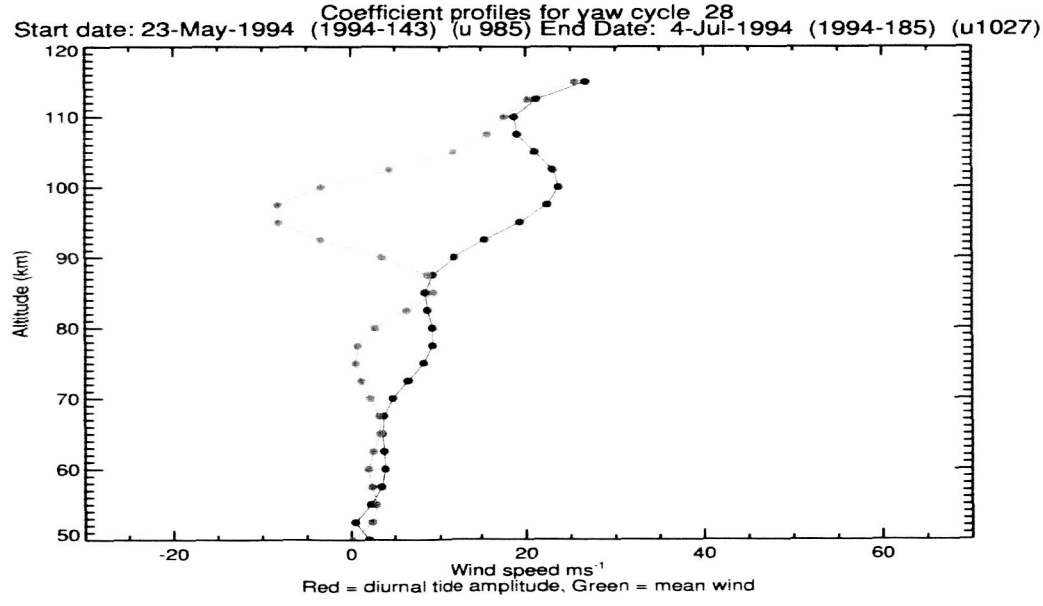

Figure 7. Fit near solstice

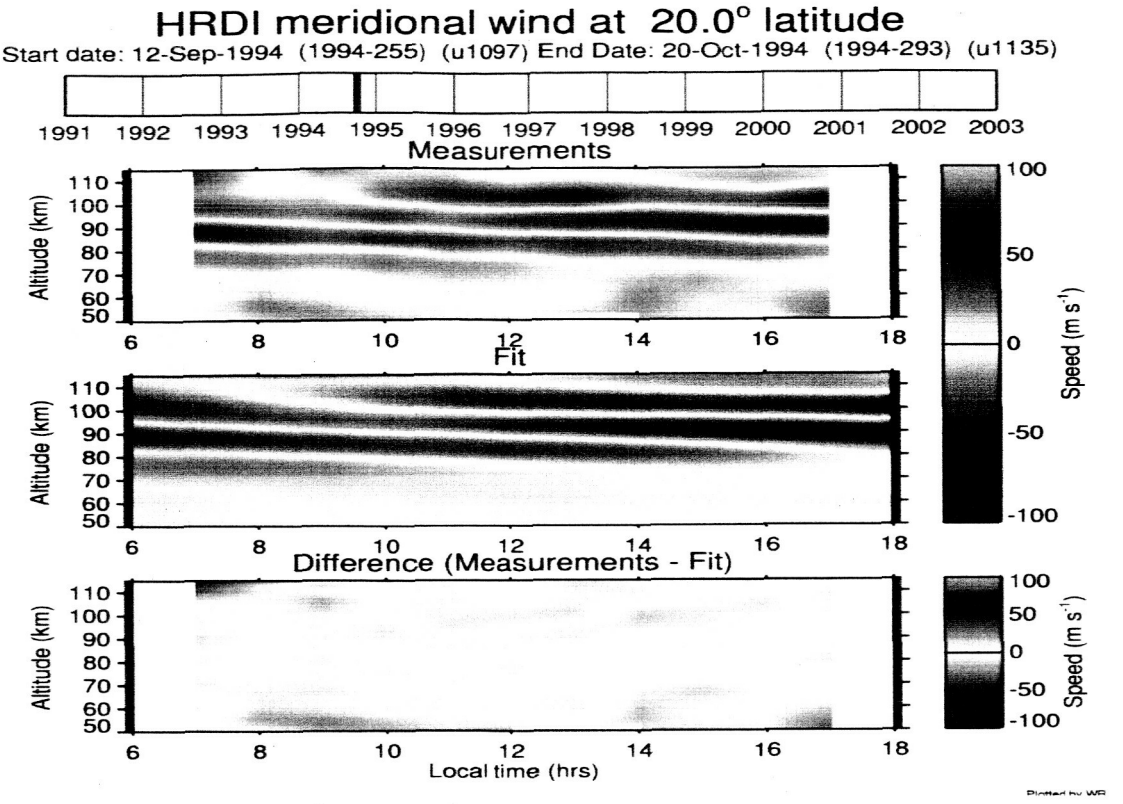

Figure 8. Meridional winds near equinox

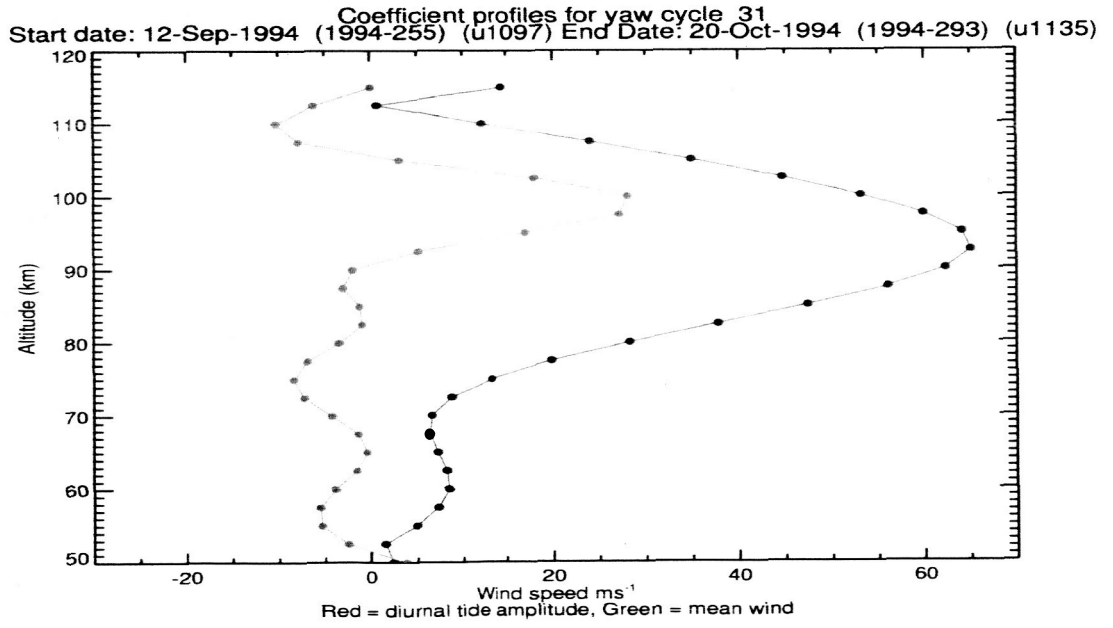

Figure 9. Fit near equinox

The monthly values of the tidal amplitude derived were then fit to the proxy forcing functions. The tidal amplitude is assumed to be of the form

$$\text{Tide Amplitiude} = \text{Mean} + \text{Solar Forcing} + \text{QBO Forcing} + \text{Stratospheric Aerosol Forcing}$$

where the forcing functions have the form

$$\text{Mean} = a_0 + a_{\text{annual}} \cos\left(\frac{2\pi t}{365.25} + \phi_1\right) + a_{\text{semiannual}} \cos\left(\frac{4\pi t}{365.25} + \phi_2\right)$$

$$\text{Solar Forcing} = I_{F10.7}\left[b_0 + b_{\text{annual}} \cos\left(\frac{2\pi t}{365.25} + \phi_3\right) + b_{\text{semiannual}} \cos\left(\frac{4\pi t}{365.25} + \phi_4\right)\right]$$

with other terms following a similar form. Figure 10 shows the fit as a function of time and altitude for the meridional wind derived from HRDI data. The semiannual nature of the tidal amplitude is clear as is quite noticeable intra-annual variations.

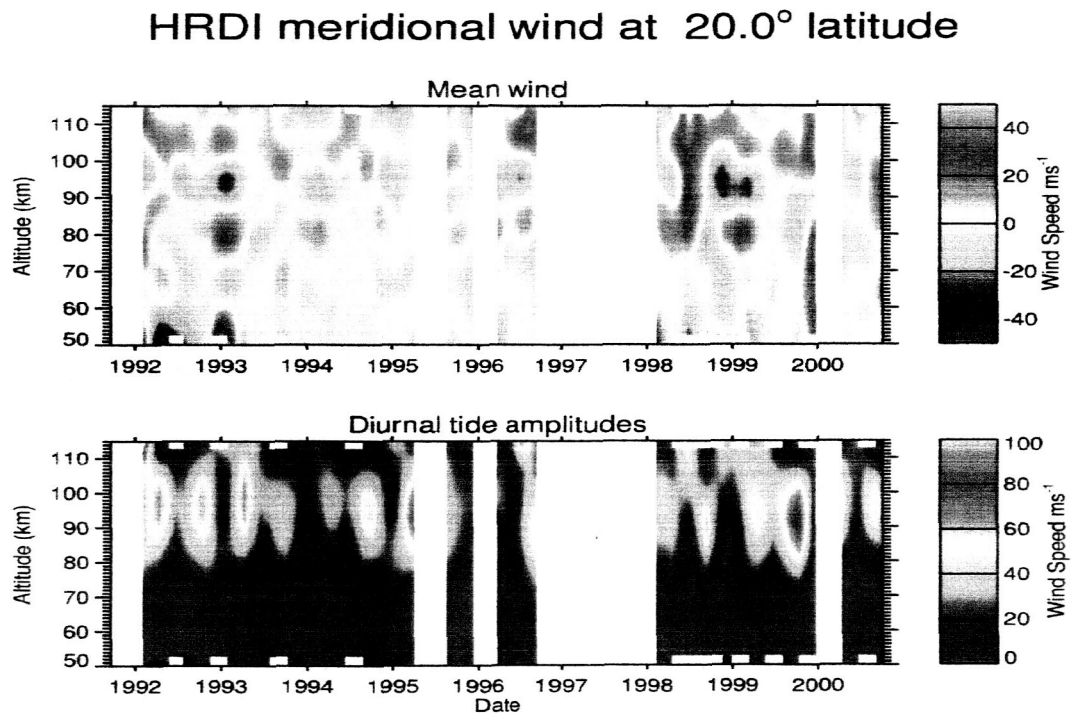

Figure 10. Derived tides and mean wind from HRDI data from 1992 to 2001.

Figure 11 shows the fit of the tidal amplitude and the measured values. This simple model captures much of the intra-annual variability seen in the data.

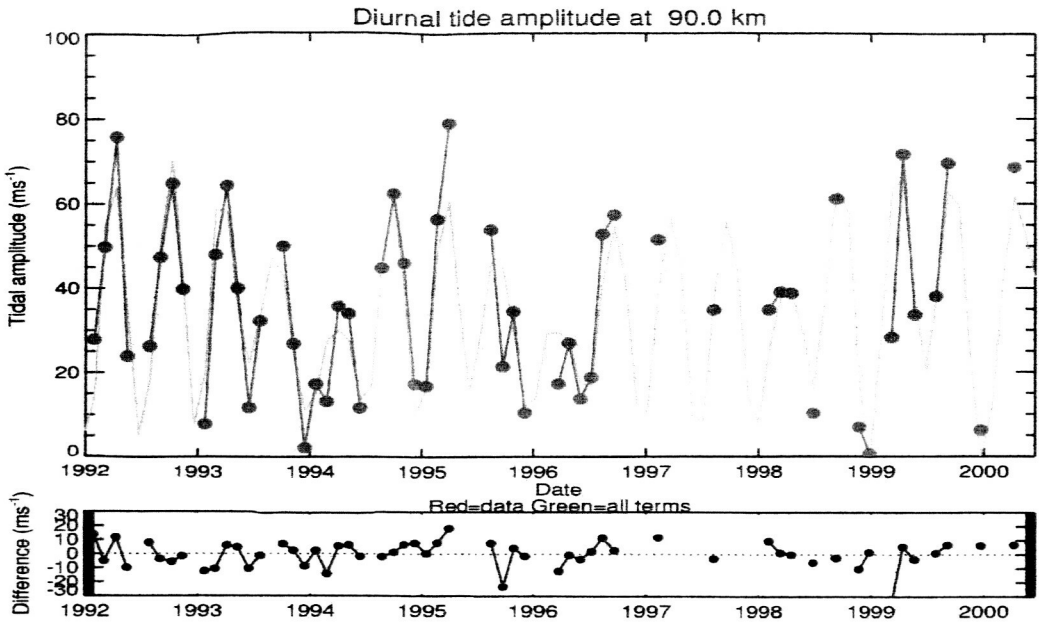

Figure 11. Tidal amplitude fit with solar, QBO and stratosphere aerosol forcing

References

Papers and Talks supported by this proposal

Hagan, M. E., M. D. Burrage, J. M. Forbes, J. Hackney, W. J. Randel, X. Zhang, "QBO effects on the diurnal tide in the upper atmosphere," Earth Planets Space, 51, 571-578, 1999.

D. Ortland, Analysis of Tempertures and Winds in the MLT measured by HRDI, Fall AGU, 1997, San Francisco.

D. Ortland, Analysis of Tempertures and Winds in the MLT measured by HRDI, UARS science team meeting, Pasadena, 1998.

D. Ortland & T. Dunkerton, HRDI measurements of temperature inversions in the upper mesosphere, Fall AGU 1998, San Francisco.

D. Ortland, A Data Assimilation Technique for Determining Tidal and Zonal Mean Structure from Satellite Measurements in the Mesosphere and Lower Thermosphere, AMS Middle Atmosphere meeting, 2000.

W. Skinner, The Mesosphere and Lower Thermosphere Wind Field Since 1991 as Observed by UARS/HRDI, COSPAR 2002, Houston.

REFERENCES

1. Burrage, M. D., M. E. Hagan, W. R. Skinner, D. L. Liu, and P. B. Hays, "Long-term variability in the solar diurnal tide as observed by HRDI and simulated by the GSWM, " Geophys. Res. Lett., 22, 2641-2644, 1995.
2. Burrage, M. D., D. L. Wu, W. R. Skinner, D. A. Ortland, and P. B. Hays, "Latitude and seasonal dependence of the semidiurnal tide observed by the High Resolution Doppler Imager," J. Geophys. Res., 100, 11313-11321, 1995.

3. Burrage, M. D., R. A. Vincent, H. G. Mayr, W. R. Skinner, N. F. Arnold, and P. B. Hays, "Long-term variability in the equatorial mesosphere and lower thermosphere zonal wind," J. Geophys. Res., 101, 12847-12854, 1996.
4. Hagan, M. E., M. D. Burrage, J. M. Forbes, J. Hackney, W. J. Randel, X. Zhang, "QBO effects on the diurnal tide in the upper atmosphere," Earth Planets Space, 51, 571-578, 1999.
5. C. A. Reber, "The Upper Atmosphere Research Satellite," *EOS. 71*, No. 51, pp. 1867-1878, 1990.
6. M. R. Schoeberl, A. R. Douglass, and C. H. Jackman, "Overview and highlights of the UARS mission," SPIE Vol. 2266, pp. 254-265, 1994.
7. P. B. Hays, "High-resolution optical measurements of atmospheric winds from space. 1: Lower atmosphere molecular absorption," *Appl. Opt 21*, pp. 1136-1141, 1982.
8. V. J. Abreu, A. Bucholtz, P. B. Hays, D. A. Ortland, W. R. Skinner, and J.-H. Yee, "Absorption and emission line shapes in the O_2 atmospheric bands: Theoretical model and limb viewing simulations," *Appl. Opt 28*, pp. 2128-2137, 1989.
9. P. B. Hays and V. J. Abreu, "Absorption line profiles in a moving atmosphere: A single scattering linear perturbation theory," *J. Geophys. Res. 94*, pp. 18,351-18,365, 1989.
10. W. R. Skinner, P. B. Hays, H. J. Grassl, D. A. Gell, M. D. Burrage, A. R. Marshall, D. A. Ortland, "The High Resolution Doppler Imager on the Upper Atmosphere Research Satellite," in *Optical Spectroscopic Techniques and Instrumentation for Atmospheric and Space Research*, Jinxue Wang, Paul Hays, Editors, Proc. SPIE 2266, pp. 281-293, 1994.
11. W. R. Skinner, P. B. Hays, H. J. Grassl, D. A. Gell, M. D. Burrage, A. R. Marshall, and J. Kafkalidis, "The High Resolution Doppler Imager: Instrument performance in orbit since late 1991," in *Optical Spectroscopic Techniques and Instrumentation for Atmospheric and Space Research II*, Paul B. Hays, Jinxue Wang, Editors, Proc. SPIE 2830, 202-214, 1996.
12. W. R. Skinner, D. A. Gell, A. R. Marshall, P. B. Hays, J. F. Kafkalidis and D. R. Marsh, "The High Resolution Doppler Imager: Instrument performance from late 1991 to mid-1999," in *Optical Spectroscopic Techniques and Instrumentation for Atmospheric and Space Research III*, Allen Larar Editor, Proc. SPIE 3796, 304-315, 1999.
13. W. R. Skinner, A. R. Marshall, D. A. Gell, J. Raines , "The High Resolution Doppler Imager: Status update 12 years after launch," in *SPIE Conference on Optical Spectroscopic Techniques and Instrumentation for Atmospheric and Space Research V*, edited by Allen M. Larar, Joseph A. Shaw, and Zhaobo Sun, San Diego, Ca., SPIE **5157**, 231-241, 2003.
14. P. B. Hays, V. J. Abreu, M. E. Dobbs, D. A. Gell, H. J. Grassl, and W. R. Skinner, "The High Resolution Doppler Imager on the Upper Atmosphere Research Satellite," *J. Geophys. Res.- Atmos 98*, pp. 10,713-10,723, 1993.
15. H. J. Grassl, W. R. Skinner, P. B. Hays, M. D. Burrage, D. A. Gell, A. R. Marshall, D. A. Ortland, and V. J. Abreu, "Atmospheric wind measurements with the High Resolution Doppler Imager (HRDI)," *J. Spacecraft & Rockets 32*, pp. 169-176, 1995.